Environmental Pollution 255 (2019) 113182

Contents lists available at ScienceDirect

Environmental Pollution

journal homepage: www.elsevier.com/locate/envpol

Applicability of $BaTiO_3$/graphene oxide (GO) composite for enhanced photodegradation of methylene blue (MB) in synthetic wastewater under UV–vis irradiation☆

Zhu Mengting[a, 1], Tonni Agustiono Kurniawan[a, *, 1], Song Fei[a], Tong Ouyang[a], Mohd Hafiz Dzarfan Othman[b], Mashallah Rezakazemi[c], Saeed Shirazian[d]

[a] *Key Laboratory of the Coastal and Wetland Ecosystems (Xiamen University), Ministry of Education, College of the Environment and Ecology, Xiamen University, Xiamen 361102, Fujian, China*
[b] *Advanced Membrane Technology Research Centre (AMTEC), School of Chemical and Energy Engineering, Universiti Teknologi Malaysia, 81310 Skudai, Johor, Malaysia*
[c] *Faculty of Chemical and Materials Engineering, Shahrood University of Technology, Shahrood, Iran*
[d] *Department of Chemical Sciences, Bernal Institute, University of Limerick, Limerick, Ireland*

ARTICLE INFO

Article history:
Received 23 April 2019
Received in revised form
27 August 2019
Accepted 4 September 2019
Available online 7 September 2019

Keywords:
Advanced oxidation process
Dye
Refractory pollutant
Textile wastewater
Water treatment

ABSTRACT

Methylene blue (MB) is a dye pollutant commonly present in textile wastewater. We investigate and critically evaluate the applicability of $BaTiO_3$/GO composite for photodegradation of MB in synthetic wastewater under UV–vis irradiation. To enhance its performance, the $BaTiO_3$/GO composite is varied based on the $BaTiO_3$ weight. To compare and evaluate any changes in their morphologies and crystalline structures before and after treatment, BET (Brunauer–Emmett–Teller), XRD (X-ray diffraction), FTIR (Fourier transform infrared spectroscopy), SEM (scanning electron microscopy) and TEM (transmission electron microscopy) tests are conducted, while the effects of reaction time, pH, dose of photocatalyst and initial MB concentration on its photodegradation by the composite are also investigated under identical conditions. The degradation pathways and removal mechanisms of MB by the $BaTiO_3$/GO are elaborated. It is evident from this study that the $BaTiO_3$/GO composite is promising for MB photodegradation through ·OH. Under optimized conditions (0.5 g/L of dose, pH 9.0, and 5 mg/L of MB concentration), the composite with 1:2 dose ratio of $BaTiO_3$/GO has the highest MB degradation rate (95%) after 3 h of UV vis irradiation. However, its treated effluents still could not comply with the discharge standard limit of less than 0.2 mg/L imposed by national environmental legislation. This suggests that additional biological treatments are still required to deal with the remaining oxidation by-products of MB, still present in the wastewater samples such as 3,7-bis (dimethyl-amino)-10H-phenothiazine 5-oxide.

1. Introduction

In recent years, China's rapid industrialization have led to an increasing water consumption in dye-related industries such as textile (Jiang, 2009). Such industries contribute to large amounts of wastewater laden with dye pollutants including MB. It is estimated that textile printing and dyeing (TPD) industry has a major share up to approximately 40% of the total industrial wastewater discharge nationwide with its daily emission ranging between 3×10^6 m^3/d and 4×10^6 m^3/d (Lin et al., 2018a). The TPD wastewater, characterized by a high concentration of refractory pollutants such as MB, is difficult to be treated (Wang et al., 2001), as its dark color continually absorbs sunlight in tropical regions, causing hazardous effects to aquatic organisms. Hence, it is quite complicated and costly to remove both the pollutant and its color from such wastewater in large-scale water treatment plants (Mohtora et al., 2018).

Although MB is not toxic, when it is ingested higher than 7.0 mg/

☆ This paper has been recommended for acceptance by Baoshan Xing.
* Corresponding author.
E-mail address: tonni@xmu.edu.cn (T.A. Kurniawan).
[1] The first and the second authors equally contribute to this article and share the first authorship.

https://doi.org/10.1016/j.envpol.2019.113182
0269-7491/

kg, this can cause health disorders such as high blood pressure, nausea, and abdominal pain (Oz et al., 2011). Moreover, the MB can be freely photosensitized by light to produce hazardous oxygen ($^1O_2$) (Albadarin et al., 2017a), which can damage our DNA structure, especially when being present in high concentrations (Carneiro et al., 2010). Unless treated, the discharge of the MB pollutant into a water body would affect the surrounding aquatic environment and public health. Therefore, it is necessary to treat the wastewater laden with MB.

Various water technologies, including reverse osmosis (Chan et al., 2007) and adsorption (Babel and Kurniawan, 2003, 2004; Lin et al., 2018b), have been tested and developed in laboratory-settings to address global water pollution problems. However, those techniques have bottlenecks in their practical applications, such as high energy consumption, costly operational cost, and low removal efficiencies (Albadarin et al., 2017b; Fu et al., 2017). As a result, we need to develop state-of-the-art of environmental technologies with a unique capability of removing target pollutants indiscriminately within a short time.

Recently, photocatalytic technology has gained popularity for its novel applications in removing rhodamine B (RhB) (Sabarish and Unnikrishnan, 2018), methyl orange (MO) (Zhai et al., 2018), and MB (Banerjee et al., 2018) from wastewater. In this particular technology, photocatalysts such as TiO_2 play roles in the degradation processes through the formation of $\cdot OH$ (Vig et al., 2018). The $\cdot OH$ rapidly attacks target pollutant and degrades it completely into CO_2 and H_2O under UV−vis irradiation (Fig. S1) (Jilani et al., 2018).

Among a variety of photocatalysts, $BaTiO_3$, due to its excellent dielectric, ferroelectric, and piezoelectric properties (Gromada et al., 2017; Rezakazemi et al., 2018), has potentials for applications in optoelectronic devices. However, the photocatalyst with 3.25 eV of band gap has a weak light response range, which inhibits its applications for water treatment. In addition, the wide band gap of the $BaTiO_3$ makes it unable to utilize the UV−vis effectively due to its fast recombination rate caused by the semiconductor's electron-hole pairs (e^-, h^+) (Azarang et al., 2014, 2018). Such drawbacks would hinder it from having an efficient photodegradation. To address these bottlenecks, innovative technological approaches such as surface sensitization (Li et al., 2015), morphological control (Sahu et al., 2019), ion doping (Hong et al., 2018), noble metal loading (Ramezanpour et al., 2018), and construction of hetero-structure (Yan et al., 2010), have been developed recently to mitigate the impacts attributed to them.

A number of previous studies reported that the use of $BaTiO_3$ for photodegradation could remove diclofo-*p*-methyl and dyes (Devi and Krishnamurthy, 2009; Nageri and Kumar, 2018). Li et al. (2013b) found that the electron-hole pairs (e^-, h^+) of the $BaTiO_3$ migrate to its conduction band during reaction, and then produce $\cdot O^-{}_2$ to degrade the MB (Reactions (1)–(3)) (Yang et al., 2005). However, only 64% of MB removal was achieved by the $BaTiO_3$ alone with an initial MB concentration of 5 mg/L.

$$BaTiO_3 \rightarrow_{h\nu} BaTiO_3\left(e^-_{cb} + h^+_{vb}\right) \tag{1}$$

$$e^-_{cb} + O_{2\,(adsorbed)} \rightarrow \cdot O_2^-\,(adsorbed) \tag{2}$$

$$e^-_{cb} + h^+_{vb} \rightarrow heat \tag{3}$$

To address the bottlenecks caused by its wide bandgap, in this study, the $BaTiO_3$ was integrated with graphene oxide (GO), a single monolayer of graphite with oxygenated functional groups like hydroxyl groups, carbonyl, epoxide and carboxyl, as a hybrid composite. It is expected that the new composite that consisted of both $BaTiO_3$ and GO would have unique physical, chemical, optical and mechanical properties (Han et al., 2014, 2016) with a shorter bandgap than that of the $BaTiO_3$, one of its starting compounds. The GO is a useful loading material because it may have the ability to play unique roles as a macromolecular photosensitizer that act as a reservoir of electrons to shuttle the electrons generated from the $BaTiO_3$ (Zhang et al., 2012; Fu et al., 2019). The GO may form a unique composite with the $BaTiO_3$ for enhancing MB photodegradation under UV−vis irradiation, as the composite may possess ferroelectric properties coupled with large active sites with a shorter bandgap.

In addition, the GO has a large specific surface area (500−1200 m^2/g) (Dervin et al., 2017) that act as active sites for photocatalytic degradation applications (Wang et al., 2014), while the $BaTiO_3$ can be uniformly anchored at the active sites of the GO in the form of composite (Liu et al., 2016, 2017). The hydroxyl or carboxyl groups of the GO may promote the formation of a steady structure of the $BaTiO_3$/GO composite for photodegradation. Both $BaTiO_3$ and GO are complement to each other, as in the form of composite, their hybrid not only increases the transfer of electrons between them, but also decreases the recombination rate of their hole-electron pairs (Xu et al., 2013), improving photodegradation efficiency.

A previous study carried out by Kurniawan et al. (2018) reported the feasibility of the $TiO_2/BaTiO_3$ composite for acetaminophen removal from aqueous solutions. Separately Ong et al. (2019) revealed that a photoanode with 1:1 dose ratio of $BaTiO_3$/ZnO exhibited the highest photocatalytic activity for the degradation of RR120 in aqueous solutions. In spite of unique physico-chemical properties of the $BaTiO_3$, to the best of authors' knowledge, studies on the synthesis, characterization, and application of the $BaTiO_3$/GO composite for MB removal have so far been rarely reported in the body of knowledge (Lin et al., 2017; Zhao et al., 2018).

In this study, we investigate the applicability and performance of the $BaTiO_3$/GO composite for photodegradation of MB in synthetic wastewater under UV−vis irradiation. To enhance its removal performance, the $BaTiO_3$/GO composite is varied based on the $BaTiO_3$ weight. To compare and evaluate changes in their morphologies and crystalline structures before and after treatment, BET, XRD, FTIR, SEM and TEM tests are conducted, while the effects of reaction time, pH, dose of photocatalyst and initial MB concentration on its photodegradation by the same composite are investigated. The degradation pathways and the mechanisms of the MB removal by the $BaTiO_3$/GO are also elaborated in this study.

2. Materials and methods

2.1. Materials

$BaTiO_3$ with 99.9% purity was obtained from Aladdin Reagent Co. (Shanghai, China). Natural graphite, supplied by the same supplier, was used to prepare the GO through the modified Hummer's method, as reported by Li et al. (2013a). Methylene blue, used in its as-received form, was provided by Acros (New Jersey, US) (Table S1). The stock solution of MB was prepared by dissolving 1 g of the chemical in 1 L of deionized water. Working solutions were freshly prepared by diluting the same stock solution to pre-determined concentrations from 2.5 to 20 mg/L. The pH-meter (FE 20, Switzerland) was used to adjust the pH of the synthetic dye wastewater by 1.0 M HCl and/or NaOH.

2.2. Methods

2.2.1. Synthesis of single layer GO

In this study, the GO sheet was synthesized based on the modified Hummers' method (Li et al., 2013a). Initially, 2.50 g of graphite and 1.25 g of $NaNO_3$, respectively, were added into 70 mL of 1 M H_2SO_4. The mixture was stirred at 278 K. Subsequently, about 7.50 g $KMnO_4$ were added into this mixture, while maintaining the same temperature for 6 h. The temperature of the suspension was then increased to 393 K and stirred for 30 min. The solution was cooled down at ambient temperature and then 25 mL of H_2O_2 was added into the suspension to terminate the reactions. The suspension was centrifuged and washed with 5% HCl and deionized water until the pH was 7. The resulting GO was obtained by applying ultrasonic dispersion of the suspension and dried in an oven at 378 K for 24 h.

2.2.2. Synthesis of $BaTiO_3$/GO composite

A predetermined amount of $BaTiO_3$ and GO, respectively, were added into 0.1 L of ethanol solution, and stirred for 1 h at ambient temperature. The weight ratio between the $BaTiO_3$ and the GO was varied based on the weight of $BaTiO_3$ (Table S2).

The mixture was then transferred to a polytetrafluoroethylene reactor and put in an oven at 473 K for 3 h. After the reaction was complete, the mixture was cooled down to ambient temperature and filtered. Subsequently, the composite was repeatedly washed using 70% (v/v) ethanol. The obtained composites were washed and filtered using distilled water and ethanol until the pH of the solution was 7.0. Finally, the composites were dried in an oven at 333 K for 48 h to obtain the $BaTiO_3$/GO composites with varying dose ratios. The overall synthesis process of the composite is presented in Fig. S2.

2.2.3. Characterization of $BaTiO_3$/GO composite

To detect any changes in their crystalline forms after treatment, XRD (model Rigaku Ultima IV, Tokyo) tests were employed to analyze their phase composition. The equipment was operated at 40 kV and 30 mA from a range of 5°–60° at 10°/min of scanning speed. To identify the presence of functional groups in the composites, FTIR studies were conducted. To determine their degree of dispersion between the particles, agglomeration, grain size and shape, the morphology and microscopic structures of the composites were studied by using a SEM (model ZEISS SIGMA, Germany), which operated at 15 kV, while their microstructures were analyzed using a TEM (model Tecnai F30, the Netherlands). A UV–vis spectrophotometer (model UV-1800PC, Mapada, Shanghai), was used to determine the remaining MB concentrations after treatment.

2.2.4. Photocatalytic degradation

A cylindrical reactor with a height of 220 mm and a diameter of 10 mm was used in this study. The volume of the photoreactor was 0.5 L, which contained both target contaminant and the photocatalyst. The experiments were conducted at ambient temperature (Fig. S3).

In this treatment, the photocatalyst was dispersed in 500 mL of MB solution with continuous stirring throughout the experiments. The reaction was kept in the dark for 30 min to establish adsorption–desorption equilibrium in the reactor. To maximize the removal of MB in aqueous solutions, parameters such as reaction time, pH, dose of photocatalyst, and initial MB concentration, were varied under optimized conditions. After being exposed to the UV–vis irradiation, about 5 mL of samples were collected from the reactor every 30 min and filtered using Millipore filter papers (with their pore size of 0.45 μm) before undertaking chemical analyses subsequently.

2.2.5. Chemical analyses of MB

After treatment, the remaining concentration of MB was determined at the maximum wavelength (λ) of 664 nm. The removal efficiency ($\eta_e(\%)$) of MB was calculated based on:

$$\eta_e(\%) = [1 - (C_e/C_0)] \times 100\% \tag{4}$$

where C_0 and C_e are the initial and the equilibrium MB concentration after treatment, respectively.

2.2.6. Statistical analysis

All the average values were obtained by undertaking the experiments in duplicate under identical conditions. The maximum coefficient of data variation was less than 5%. The statistical tests were carried out using SPSS 19.0 Windows Version with a confidence interval of 95%.

3. Results and discussions

3.1. Characterization of $BaTiO_3$/GO composites

3.1.1. BET analyses

Table S3 presents the surface areas of as-received $BaTiO_3$ and $BaTiO_3$/GO composites. It is obvious that GO doping substantially increase the S_{BET} of $BaTiO_3$/GO composites. As the GO loading into the $BaTiO_3$ increases, the pore size of the $BaTiO_3$/GO composites decrease.

The S_{BET} of the as-received GO was 500–1200 m^2/g (Dervin et al., 2017), while that of the $BaTiO_3$/GO-33% is the largest (62 m^2/g). It was anticipated that the GO doping on the $BaTiO_3$ might enlarge the surface area of the composites formed. Hence, the increasing surface areas of the composites not only would promote photocatalytic activities, but also provide additional active sites for reacting with the target pollutant (Benjwal and Kamal, 2015).

3.1.2. XRD analyses

Fig. 1 shows the crystal structures of pure $BaTiO_3$, GO as well as the $BaTiO_3$/GO-20%, 33%, 66%, 80% composites.

The characteristic peak of the GO, which appears at around 10.5°, indicates the presence of its ordered layered structure (Yao et al., 2013), while the peaks of all the composites at the same degree suggested that the GO was successfully doped into the $BaTiO_3$. As reflected by all the composites, the higher the ratio of the doped GO into the composites is, the sharper their peaks are. The peaks of all the composites, which appear at 21.9°, 31.4°, 38.8°,

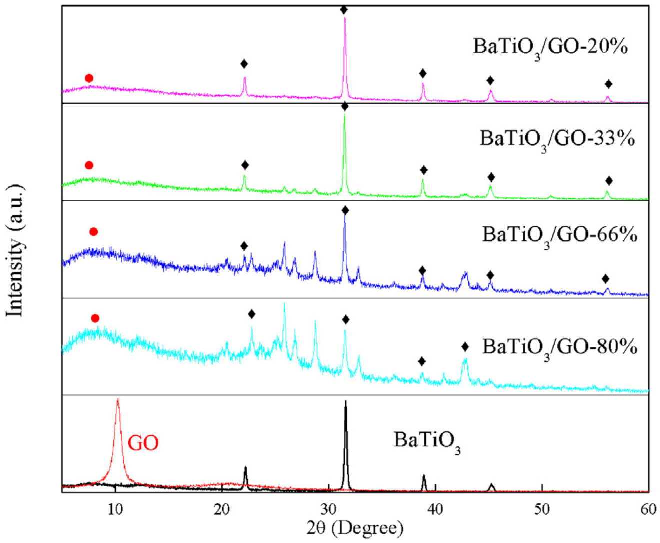

Fig. 1. XRD patterns for various types of $BaTiO_3$/GO composites.

45.1°, 51.1°, 56.1°, and 65.7°, suggest their good crystallinity. The characteristic peaks' position of the $BaTiO_3$ remained unchanged in other composites, reflecting that its crystal structure also remained present in the composites.

It is important to note that the presence of the GO in the crystalline structure of the composite might have changed the electronic structure of the composite's *C* orbitals with its energy lower than that of the *Ti* orbitals in its conduction band (*cb*). Consequently, this not only shortened its bandgap, but also slowed down its recombination rate and exposed the photocatalyst to the UV–vis effectively for an efficient photodegradation. These findings were in agreement with those of Lacerda and de-Lazaro (2016), who reported that a Zn-doping process into $BaTiO_3$ had significantly reduced the bandgap in its conduction band (*cb*).

Fig. 1 also shows that in the XRD patterns of the $BaTiO_3$/GO-66% and the $BaTiO_3$/GO-80% composites, we observed several peaks other than the pure $BaTiO_3$. Those peaks are impurity due to the addition of GO into the $BaTiO_3$. The higher the content of the GO doped with $BaTiO_3$ was, the lower the crystallinity of the composites was, resulting in additional peaks during the XRD analyses.

Due to their higher peaks, it is obvious that both the $BaTiO_3$/GO-20% composite and the $BaTiO_3$/GO-33% composites had better crystallinity properties and larger crystal grains than did the $BaTiO_3$/GO-66% composite and the $BaTiO_3$/GO-80% composite. As the ratio of GO in the composites increased, the intensity of the GO was enhanced, while the intensity of the $BaTiO_3$ decreased. These results confirmed those of Yao et al. (2013), who reported the $BaTiO_3$/GO composites displayed mixed $BaTiO_3$ and GO diffractions due to varying intensities.

3.1.3. FTIR analyses

The FTIR spectra of GO, pure $BaTiO_3$ and the $BaTiO_3$/GO-20%, 33%, 66%, 80% samples are presented in Fig. 2. The FTIR spectra of the GO revealed unique absorptions due to the presence of C–O group in 500–1000 cm^{-1}, while the stretching vibration at 1300 cm^{-1} was attributed to the C–O–C group and the one in 1600 cm^{-1} was related to the C–O–H group. Furthermore, the O–H stretching vibration, which existed at 3400 cm^{-1}, revealed a strong and broad absorption peak of the GO. These results indicated various types of oxygen functionalities present on its surface (Szabo et al., 2006).

The bands located at 3480, 2900, 2800 and 1628 cm^{-1} were attributed to the O–H group's vibration stretching because of the water molecules present on the surfaces of the $BaTiO_3$ (Jung et al., 2005; Utara and Hunpratub, 2018; Zheng et al., 2013). As reflected by their FTIR spectra, the peaks of the O–H, C=O, and C–O groups of the four composites still exist in the same range of the bands belong to the composites, as reported by Ran et al. (2019). This suggests that the physico-chemical characteristics of the GO might not change after being integrated with $BaTiO_3$ as a composite.

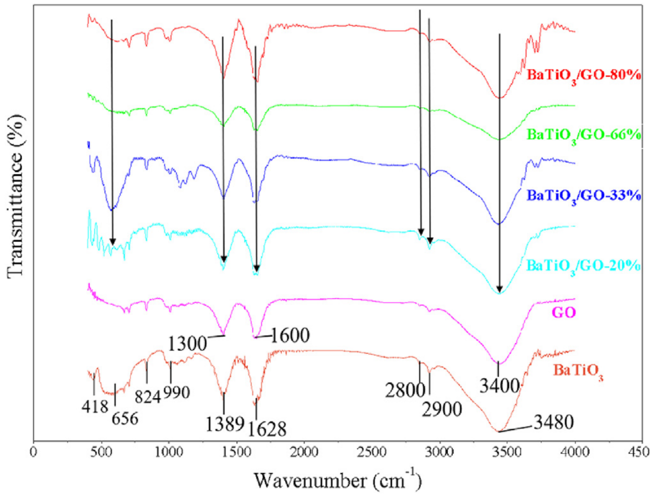

Fig. 2. FTIR spectra of GO, pure $BaTiO_3$ and various $BaTiO_3$/GO composites.

3.1.4. SEM and TEM analyses

The surface morphologies of GO, pure $BaTiO_3$ and $BaTiO_3$/GO composites are presented in Fig. 3. Fig. 3a presents a spherical $BaTiO_3$ with its core-shell structure that has a homogeneous grain size, while Fig. 3b–e depicts that the GO sheets were wrinkled, where the $BaTiO_3$ particles were attached to its surface. However, the GO-doped $BaTiO_3$ did not have any effects on the spherical morphology of the $BaTiO_3$. Fig. 3b–e indicate that the $BaTiO_3$/GO composites were synthesized successfully. This finding affirmed earlier findings reported by Vasilaki et al. (2015), who found that the nanoparticles tended to accumulate along the wrinkles of the GO sheets.

Although all of the composites have GO content, the $BaTiO_3$/GO-66% composite might have had the highest photocatalytic activity, as compared to the others. The obvious difference between this $BaTiO_3$/GO-66% composite and others was that the $BaTiO_3$ particles were distributed more uniformly in the $BaTiO_3$/GO-66% than those in the other composites (Fig. 3d). This enabled the $BaTiO_3$/GO-66% to have enhanced photocatalytic activities under UV–vis irradiation.

As presented in Fig. 4a, the TEM images of the GO sample depicts obvious wrinkles on its surface, typical features of monolayer graphene (Meyer et al., 2007), while Fig. 4b shows that the surface of the GO sheet was uniformly covered with the $BaTiO_3$. The $BaTiO_3$ had homogeneous particle dispersions on the GO surface, an essential factor for enhanced photocatalytic performance.

3.2. Photodegradation studies

3.2.1. Control study without photocatalysts

For control study, an aqueous system without any photocatalyst was irradiated under UV–vis light. After 4 h of irradiation, the MB removal was negligible (1.1% of MB removal with its initial concentration of 5 mg/L). On the other hand, under 4 h of UV–vis irradiation, only 3.2% of the MB could be removed by the $BaTiO_3$ alone under the same concentration of 5 mg/L at pH 9.0 (Fig. 5). To enhance its removal performance for water treatment applications, therefore, it is necessary to integrate both the $BaTiO_3$ and the GO as a composite.

3.2.2. Effects of reaction time on MB removal

Fig. 5 presents the MB removal by various composites under UV–vis irradiation for 4 h. The MB removal improved gradually with an increasing time and eventually reached an equilibrium state at a certain time. The four composites have higher MB removal efficiencies than the $BaTiO_3$ alone as follows: $BaTiO_3$/GO-66% composite (94.57%) > $BaTiO_3$/GO-80% composite (94.09%) > $BaTiO_3$/GO-20% composite (88.61%) > $BaTiO_3$/GO-33% composite (88.52%), respectively. Due to its highest removal efficiency, the $BaTiO_3$/GO-66% composite was used for subsequent experiments.

Fig. 5 indicated that an increasing GO doping ratio promoted a higher photocatalytic activity. The optimum condition of the $BaTiO_3$/GO (w/w) ratio was 1:2. This result could be explained due to the fact that the larger specific surface area of the $BaTiO_3$/GO composite has, the more active sites it possesses, decreasing the possibility of its electron-pairs recombination. This finding is in

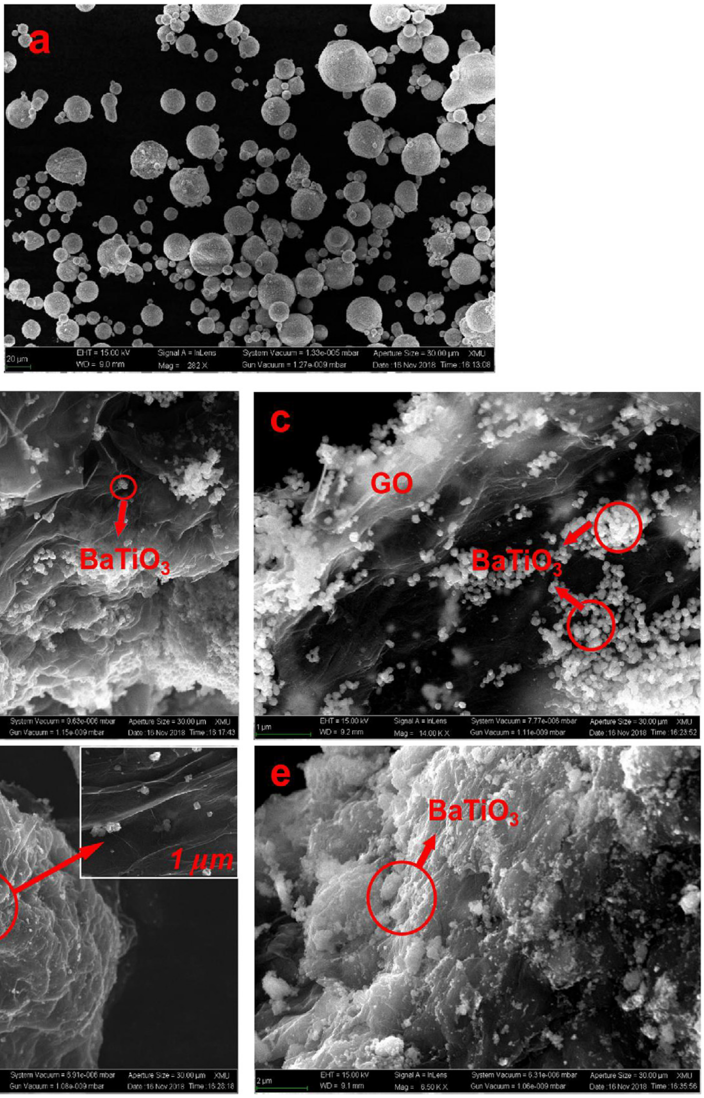

Fig. 3. SEM images of (a) pure $BaTiO_3$ (b) $BaTiO_3$/GO-20% composite (c) $BaTiO_3$/GO-33% composite (d) $BaTiO_3$/GO-66% composite and (e) $BaTiO_3$/GO-80% composite.

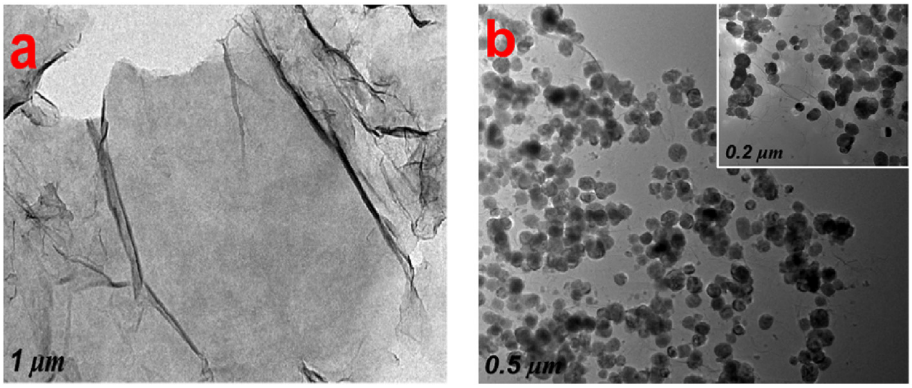

Fig. 4. TEM images of GO alone and/or $BaTiO_3$/GO-66% composite.

agreement with that of Sharma et al. (2018), who found that the GO-doped photocatalyst enhanced the charge separation and extended the increment in its surface area for promoting a higher dye adsorption.

3.2.3. *Effects of pH on MB removal by $BaTiO_3$/GO composite*

pH affects not only the charge properties of the photocatalyst and charge distribution on its surface, but also electrostatic interactions between adsorbate and the photocatalyst in aqueous

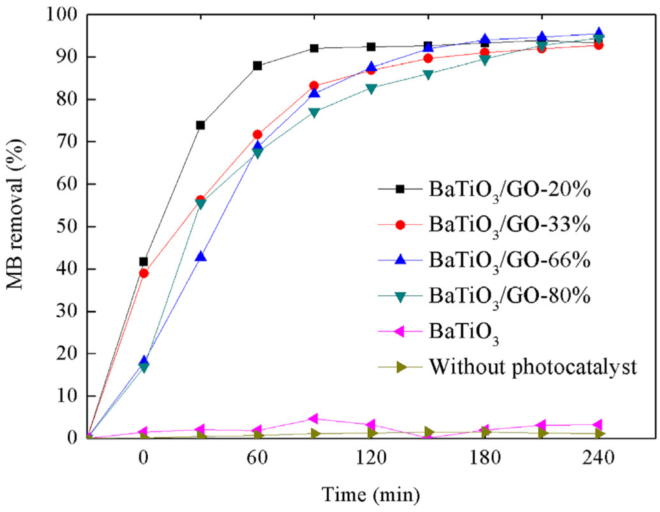

Fig. 5. Photodegradation efficiencies of MB with varying ratios of $BaTiO_3$/GO composite (concentration of MB: 5 mg/L, dose of photocatalyst: 0.5 g/L, pH 9, reaction time: 4 h, 25 °C).

solutions (Kurniawan et al., 2006a; Kurniawan and Lo, 2009). Therefore, it is necessary to determine an optimum pH. For this reason, the pH was varied from 3 to 11 during the photodegradation reaction using the $BaTiO_3$/GO-66% composite under UV–vis irradiation (Fig. 6). The results show that a maximum removal of MB was attained at pH 9 after 4 h of reaction with its initial concentration of 5 mg/L.

We also tested it with 10 mg/L of MB concentration to confirm pH dependence of MB photodegradation by the composite at a higher MB concentration. Similar results of pH dependence on MB concentration are presented in Fig. 6b.

Under the same conditions, MB removal gradually increased when the pH was increased from 3 to 9. At pH 9 (alkaline environment), the isoelectric point of the $BaTiO_3$/GO-66% composite increased because at the equipotential point, the surface charge of the photocatalyst trapped electron-hole pairs on the $BaTiO_3$/GO's surface and reduced the recombination probability of electron-hole pairs, thus enhancing its photocatalytic activity for an efficient MB photodegradation. This result confirmed earlier findings reported by Zhu et al. (2005) and Eskelinen et al. (2010), who reported that an alkaline environment was suitable for the photocatalytic oxidation of target pollutants under UV–vis irradiation.

For this reason, the MB removal by the composite was higher in alkaline conditions (pH 9) than that in acidic conditions because its active surface exhibited a net negative change. This facilitated attractive columbic forces between the negative surface charge of the composite and the positive charge of the MB molecules, leading to a higher dye removal (Fig. S4) (Kosmulski, 2009; Singh and Dutta, 2019). On the other hand, in acidic conditions, the net positive surface charge of the composite repelled the cations of the MB, typically a basic dye of thiazine, resulting in a lower MB removal by the composite.

Another reason that could explain this is the formation of $\cdot$OH in alkaline environment, as OH^- in basic conditions are freely react with the photogenerated holes of the $BaTiO_3$ (Reactions (5)–(6)), resulting in a higher MB degradation promoted by the $\cdot$OH (Fig. S5).

$$h^+ + OH^- \rightarrow \cdot OH \tag{5}$$

$$\cdot OH + MB \rightarrow \text{oxidation by-products} \rightarrow CO_2 + H_2O \tag{6}$$

3.2.4. *Effects of dose on MB removal*

An optimum dose of photocatalyst may enhance a photodegradation process by maximizing the absorption of radiation photons by its surface area. Fig. 7 illustrates the effects of dose on MB removal by $BaTiO_3$/GO-66% composite with varying dose from 0.05 to 0.50 g/L.

The results showed that the amount of the photocatalyst affected the decolorization of the MB in aqueous solutions. With the increasing dose of the $BaTiO_3$/GO-66% composite from 0.05 to 0.50 g/L, the MB removal was enhanced from 29% to 95%. This is significantly higher than that by the $BaTiO_3$ alone (3.1%) under the same optimum conditions (0.5 g/L of $BaTiO_3$; pH 9.0; 5 h of reaction time; MB concentration of 5 mg/L) ($p \leq 0.05$; *t-test*). This suggests the $BaTiO_3$/GO composite has a higher MB photodegradation than the $BaTiO_3$ alone due to its lower recombination rate (e^-/h^+ pairs). Wang et al. (2015) reported that there was an obvious red shift in the absorption edge of the composite in the visible region. Due to the presence of the –OH, C=O and –COO- groups (Section 3.1.3) on the surface of GO, the $BaTiO_3$/GO composite might have new

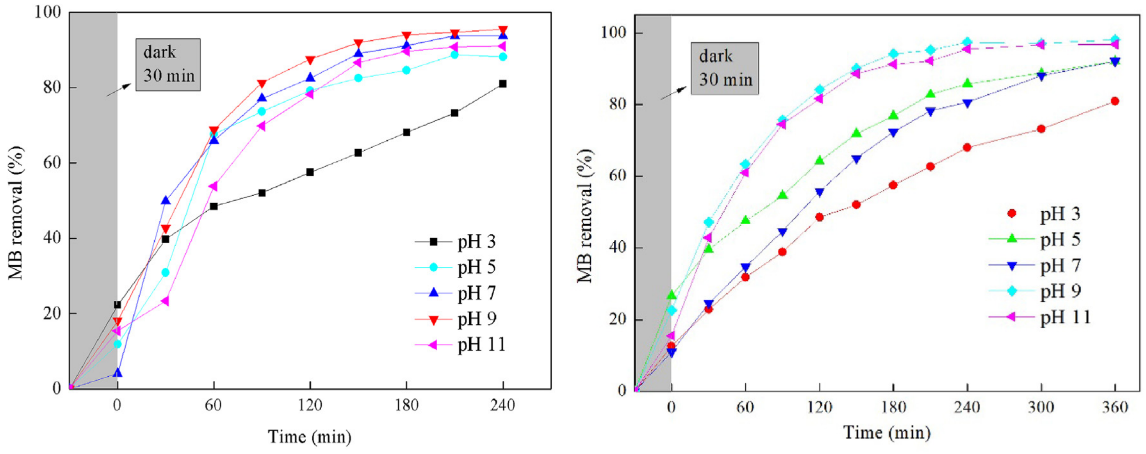

(a) At 5 mg/L of MB concentration **(b)** At 10 mg/L of MB concentration

Fig. 6. Effects of pH on MB degradation (dose of photocatalyst: 0.50 g/L, reaction time: 4 h, 25 °C).

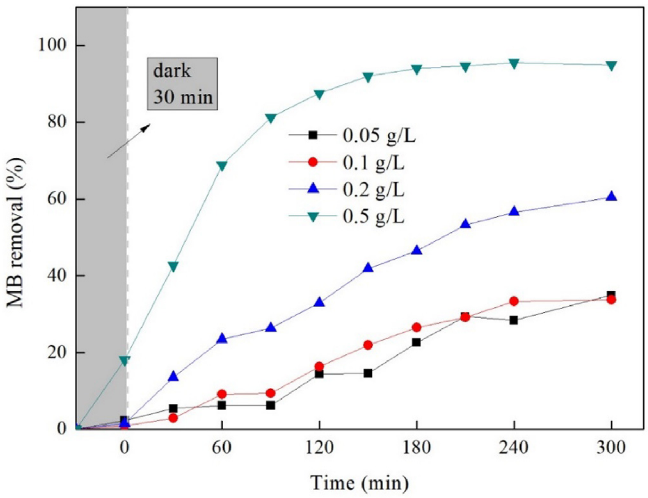

Fig. 7. Effects of photocatalyst's dose on MB degradation by $BaTiO_3$/GO-66% composite (concentration of MB: 5 mg/L; pH 9; reaction time: 5 h; 25 °C).

physico-chemical characteristics, as reflected by its shorter bandgap ($E_g = 2.56$ V) than that of the $BaTiO_3$ alone ($E_g = 3.25$ V), as indicated by earlier XRD results (Section 3.1.2).

When the dose of the composite was low, it could not provide enough active sites for reacting with target pollutants, leading to a slow reaction rate and a low MB removal by the photocatalyst. This result is in agreement with those of previous studies, which reported the importance of an optimum dose of the photocatalyst for maximizing the photodegradation reactions (Cassano and Alfano, 2000; Favier et al., 2015; Babu et al., 2019).

3.2.5. Effects of initial MB concentration on its removal by $BaTiO_3$/GO composite

A high concentration of adsorbate in aqueous solutions may saturate the photocatalyst's surface, lowering its catalytic activity (Saquib and Muneer, 2003). The effects of initial MB concentration during photodegradation were investigated using 0.5 g/L of the $BaTiO_3$/GO-66% composite with varying MB initial concentrations from 2.5 to 20 mg/L.

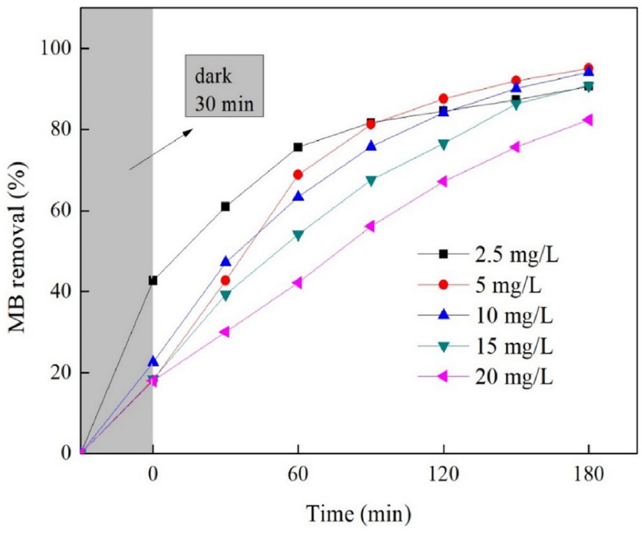

Fig. 8. Effects of initial MB concentration on its degradation rate (dose of photocatalyst: 0.50 g/L, pH 9, reaction time: 3 h, 25 °C).

Fig. 8 shows that the MB removal by the photocatalyst improved with an increasing reaction time. As the MB concentration increased, the rate of MB photodegradation gradually decreased (Bahnemann, 2004; Chong et al., 2009; Yang et al., 2019). This could be due to the fact that at a higher concentration of MB, the adsorption layer of the $BaTiO_3$/GO-66% composite became thicker, preventing the UV–vis from reaching the surface of the photocatalyst. A high concentration of the pollutant may retard the excitation of the hole-electron pair of the photocatalyst, lowering its photocatalytic activities. This result is consistent with other works undertaken by Wang et al. (2008), who found that when the target contaminant was effectively adhered to the photocatalyst's surface, the reaction would be fast and effective. The optimum MB concentration was 5 mg/L, which attained the highest MB removal (95%) under the same operating conditions.

3.3. Photocatalytic mechanisms and degradation pathways of MB removal

The photodegradation steps of MB by the composite are presented in Fig. S6. Under UV–vis irradiation, the $BaTiO_3$/GO composite excites and generates holes (h^+) and electrons (e^-). The electrons (e^-) react with the dissolved O_2 to produce $\cdot O_2^-$ (Anjaneyulu et al., 2019). Subsequently, $\cdot O_2^-$ dissociates into $HOO\cdot$. Overall, the holes (h^+) react with OH^- and H_2O and generate $\cdot OH$, which rapidly attacks the pollutant's molecule, breaking down the target pollutant into CO_2 and H_2O (Zhao et al., 2005; Kurniawan et al., 2006b; Sillanpaa et al., 2011) (Reactions (7)–(9)).

$$\cdot O_2^- + H^+ \rightarrow HO_2\cdot \tag{7}$$

$$h^+ + OH^- \rightarrow \cdot OH \tag{8}$$

$$h^+ + H_2O \rightarrow \cdot OH + H^+ \tag{9}$$

We also elaborate the MB degradation pathways by the $BaTiO_3$/GO (Fig. S7). Initially, the Cl^- is ionized and MB exists as MB^+. Afterward, there are two different paths for MB^+ to degrade. Initially, the MB^+ is attacked by $\cdot OH$ to form 3,7-bis (dimethylamino)-10H-phenothiazine-5-oxide, as reported by Ray et al. (2017). Subsequently, hydroxylation represent a further step for MB photodegradation to generate multiple single ring structures as intermediate products, as reported by Su et al. (2019). Eventually, the low molecular weight organic matter is mineralized into relatively harmless CO_2, H_2O, SO_4^{2-}, and NH_4^+ (Kurniawan et al., 2011). The degradation pathways of MB and their oxidation by-products during photodegradation have been well documented in the literatures recently (Kuan et al., 2013; Luan and Hu, 2012; Luan et al., 2015; Wolski and Ziolek, 2018).

3.4. Comparison of treatment performance by a variety of photocatalysts

To evaluate the photocatalytic activities of the $BaTiO_3$/GO composite for MB removal, it is important to compare the results of this current study to those of earlier findings reported in the body of knowledge. Operational conditions such as initial concentration, type and dose of photocatalyst, light source, reaction time as well as pH are presented in Table 1.

Table 1 summarizes the removal of organic compounds by miscellaneous photocatalysts. For example, about 64% of MB removal was attained by the $BaTiO_3$ alone with its initial concentration of 5 mg/L (Kappadan et al., 2016). The formation of the $BaTiO_3$/GO-66% composite has improved its photocatalytic activity, as the composite attained a significantly higher MB removal (95%)

Table 1
Comparison of organics removal by miscellaneous photocatalysts.

Target pollutant	Initial concentration (mg/L)	Type of photocatalyst	Dose of photocatalyst (g/L)	Light source	Light intensity (W/cm^2)	Time (min)	pH	Removal efficiency (%)	References
MB	5	$BaTiO_3$/GO-66%	0.5	Xenon	0.17	300	9	95	Present study
MB	5	$BaTiO_3$	0.5	Xenon	0.17	240	9	3	Present study
MB	5	$BaTiO_3$	0.28	Hg	NA	50	NA	64	Kappadan et al. (2016)
MB	20	$BaTiO_3$/graphene	0.67	Xenon	0.13	180	NA	93	Wang et al. (2015)
MB	10	$BaTiO_3/TiO_2$	NA	Xenon	0.10	180	NA	72	Li et al. (2013b)
MB	10	TiO_2/GO	0.2	Sunlight	NA	60	NA	95	Nguyen-Phan et al. (2011)
MB	20	TiO_2/GO	1.5	Halogen	NA	420	NA	90	Cong et al. (2013)
Ace[a]	5	$BaTiO_3/TiO_2$	1	Xenon	0.17	240	7	95	Kurniawan et al. (2018)
Ace[a]	5	TiO_2/graphene	0.1	UV	NA	180	9	96	Tao et al. (2015)
MO[b]	12	TiO_2/GO	1	Xenon	0.33	180	NA	65	Chen et al. (2010)
RhB[c]	5	$BaTiO_3$	0.33	Hg	NA	180	NA	100	Chen et al. (2016)

Remarks: NA: unavailable.
[a] Ace: Acetaminophen.
[b] MO: Methyl orange.
[c] RhB: Rhodamine.

with its initial concentration of 5 mg/L, as compared to that by the $BaTiO_3$ alone (3%) under the same optimum conditions (dose: 0.5 g/L; pH 9.0; reaction time: 5 h).

Although the use of the $BaTiO_3$/GO-66% composite as a photocatalyst was suitable to treat TPD wastewater laden with MB, their treated effluents still could not meet the increasingly strict discharge standard limit of less than 0.2 mg/L set by national legislation for dyeing wastewater. This suggests that additional biological processes are still required to deal with the remaining oxidation by-products of MB in the wastewater samples (Kurniawan et al., 2010) such as 3,7-bis (dimethyl-amino)-10H-phenothiazine 5-oxide.

4. Conclusions

This study has demonstrated that the $BaTiO_3$/GO composite is a promising photocatalyst for MB degradation from aqueous solution. Under optimized condition (0.5 g/L of dose, pH 9.0, and 5 mg/L of initial MB concentration), the composite with a 1:2 wt ratio of $BaTiO_3$/GO has the highest degradation rate for the MB. Under identical conditions, about 95% of MB degradation was attained by the same composite within 3 h of reaction time. It is important to note that the treated effluents still could not meet the increasingly strict discharge standard limit of less than 0.2 mg/L set by national legislation for this type of wastewater. This suggests that subsequent biological treatments are still required to deal with the remaining oxidation by-products of MB in the wastewater samples. The oxidation by-products of MB include 3,7-bis-(dimethylamino)-10H-phenothiazine-5-oxide and other multiple single ring structures.

Acknowledgement

The corresponding author is grateful to the World of Academy of Sciences (TWAS)' Young Affiliates Network (TYAN) and the TWAS-Elsevier Foundation, respectively, for the Collaborative Grant Award No. FR 3240304540 and the Visiting Fellowship in Sustainability No. FR 3240292438.

Appendix A. Supplementary data

Supplementary data to this article can be found online at https://doi.org/10.1016/j.envpol.2019.113182.

References

Albadarin, A.B., Solomo, S., Kurniawan, T.A., Mangwandi, C., Walker, G., 2017a. Single, simultaneous and consecutive biosorption of Cr(VI) and orange II onto chemically modified masau stones. J. Environ. Manag. 204, 365–374.

Albadarin, A.B., Charara, M., Tarboush, B.M.A., Ahmad, M.N.M., Kurniawan, T.A., Naushad, M., Walker, G., 2017b. Mechanism analysis of tartrazine biosorption onto masau stone, a low cost by-product from semi-arid regions. J. Mol. Liq. 242, 478–483.

Anjaneyulu, R.B., Mohan, B.S., Naidu, G.P., Muralikrishna, R., 2019. ZrO_2/Fe_2O_3/RGO nanocomposite: good photocatalyst for dyes degradation. Phys. E 108, 105–111.

Azarang, M., Shuhaimi, A., Yousefi, R., Golsheikh, A.M., Sookhakian, M., 2014. Synthesis and characterization of ZnO NPs/reduced graphene oxide nanocomposite prepared in gelatin medium as highly efficient photodegradation of MB. Ceram. Int. 40, 10217–10221.

Azarang, M., Sookhakian, M., Aliahmad, M., Dorraj, M., Basirun, W.J., Goh, B.T., Alias, Y., 2018. Nitrogen-doped graphene-supported zinc sulfide nanorods as efficient Pt-free for visible light photocatalytic hydrogen production. Int. J. Hydrogen Energy 43, 14905–14914.

Babel, S., Kurniawan, T.A., 2003. Low-cost adsorbents for heavy metal uptake from contaminated water: a review. J. Hazard Mater. B97, 219–243.

Babel, S., Kurniawan, T.A., 2004. Cr(VI) removal from synthetic wastewater using coconut shell charcoal and commercial activated carbon modified with oxidizing agents and/or chitosan. Chemosphere 54, 951–967.

Babu, S.G., Karthik, P., John, M.C., Lakhera, S.K., Ashokkumar, M., Khim, J., Neppolian, B., 2019. Synergistic effect of sono-photocatalytic process for the degradation of organic pollutants using CuO-TiO_2/rGO. Ultrason. Sonochem. 50, 218–223.

Bahnemann, D., 2004. Photocatalytic water treatment: solar energy applications. Sol. Energy 77, 445–459.

Banerjee, S., Benjwal, P., Singh, M., Kar, K.K., 2018. Graphene oxide (rGO)-metal oxide (TiO_2/Fe_3O_4) based nanocomposites for the removal of methylene blue. Appl. Surf. Sci. 439, 560–568.

Benjwal, P., Kamal, K.K., 2015. Simultaneous photocatalysis and adsorption based removal of inorganic and organic impurities from water by titania/activated carbon/carbonized epoxy nanocomposite. J. Environ. Chem. Eng. 3, 2076–2083.

Carneiro, C.D., Amorim, J.C., Cadena, S.M.S.C., Noleto, G.R., Di Mascio, P., Rocha, M.E.M., Martinez, G.R., 2010. Effect of flavonoids on 2'-deoxyguanosine and DNA oxidation caused by singlet molecular oxygen. Food Chem. Toxicol. 48, 2380–2387.

Cassano, A.E., Alfano, O.M., 2000. Reaction engineering of heterogeneous photocatalytic reactors. Catal. Today 58, 167–197.

Chan, G., Jie, C., Kurniawan, T.A., Fu, C., 2007. Removal of non-biodegradable compounds from stabilized leachate using VSEPRO membrane filtration. Desalination 202, 310–317.

Chen, C., Cai, W.M., Long, M.C., Zhou, B.X., Wu, Y.H., Wu, D.Y., Feng, Y.J., 2010. Synthesis of visible-light responsive graphene oxide/TiO_2 composites with p/n heterojunction. ACS Nano 4, 6425–6432.

Chen, P., Zhang, Y.T., Zhao, F.Q., Gao, H.X., Chen, X.B., An, Z.W., 2016. Facile microwave synthesis and photocatalytic activity of monodispersed $BaTiO_3$ nanocuboids. Mater. Char. 114, 243–253.

Chong, M.N., Lei, S.M., Jin, B., Saint, C., Chow, C.W.K., 2009. Optimisation of an annular photoreactor process for degradation of Congo red using a newly synthesized titania impregnated kaolinite nano-photocatalyst. Separ. Purif. Technol. 67, 355–363.

Cong, Y., Long, M., Cui, Z.W., Li, X.K., Dong, Z.J., Yuan, G.M., Zhang, J., 2013. Anchoring a uniform TiO_2 layer on graphene oxide sheets as an efficient visible light photocatalyst. Appl. Surf. Sci. 282, 400–407.

Dervin, S., Lang, Y., Perova, T., Hinder, S.H., Pillai, S.C., 2017. Graphene oxide reinforced high surface area silica aerogels. J. Non-Cryst. Solids 465, 31–38.

Devi, L.G., Krishnamurthy, G., 2009. $TiO_2/BaTiO_3$-assisted photocatalytic mineralization of diclofop-methyl on UV-light irradiation in the presence of oxidizing agents. J. Hazard Mater. 162, 899–905.

Eskelinen, K., Särkkä, H., Kurniawan, T.A., Sillanpa, M., 2010. Removal of recalcitrant contaminants from bleaching effluents in pulp and paper mills using ultrasonic irradiation and Fenton-like oxidation, electrochemical treatment, and chemical precipitation: a comparative study. Desalination 255, 179–187.

Favier, L., Simion, A.I., Rusu, L., Pacala, M.L., Grigoras, C., Bouzaza, A., 2015. Removal of an organic refractory compound by photocatalysis in batch reactor-kinetic studies. Environ. Eng. Manag. J. 14, 1327–1338.

Fu, D., Huang, Y., Zhang, X., Kurniawan, T.A., Ouyang, T., 2017. Uncovering potentials of integrated $TiO_2(B)$ nanosheets and H_2O_2 for removal of tetracycline from aqueous solution. J. Mol. Liq. 248, 112–130.

Fu, D., Kurniawan, T.A., Li, H., Wang, L., Chen, Z., Wang, H., Li, W., Wang, Y., Li, Q., 2019. Applicability of HDPC-supported Cu nanoparticles composite synthesized from unused waste digestate for octocrylene degradation in aqueous solutions. Chem. Eng. J. 355, 650–660.

Gromada, M., Biglar, M., Trzepiecinski, T., Stachowicz, F., 2017. Characterization of $BaTiO_3$ piezoelectric perovskite material for multilayer actuators. Bull. Mater. Sci. 40, 759–771.

Han, C., Yang, M.Q., Zhang, N., Xu, Y.J., 2014. Enhancing the visible light photocatalytic performance of ternary CdS-(graphene-Pd) nanocomposites via a facile interfacial mediator and co-catalyst strategy. J. Mater. Chem. A 2, 19156–19166.

Han, C., Zhang, N., Xu, Y.J., 2016. Structural diversity of graphene materials and their multifarious roles in heterogeneous photocatalysis. Nano Today 11, 351–372.

Hong, K., Cho, K.G., Lim, D.C., Lee, J.Y., Lee, K.H., 2018. Light emitting fabrics based on luminophore dye-doped ion gel electrolyte microfibers. Dyes Pigments 154, 188–193.

Jiang, Y., 2009. China's water scarcity. J. Environ. Manag. 90, 3185–3196.

Jilani, A., Othman, H.D., Ansari, O., Kumar, R., Khan, I.U., Wahab, A., Alshahrie, A., Barakat, M.A., Kurniawan, T.A., 2018. Visible light active nickel oxide@graphene oxide nanocomposite thin films: optical, dielectric, XPS surface chemical state and enhanced photocatalytic investigation. J. Mater. Sci. 53, 15034–15050.

Jung, Y.J., Lim, D.Y., Nho, J.S., Cho, S.B., Riman, R.E., Lee, B.W., 2005. Glycothermal synthesis and characterization of tetragonal barium titanate. J. Cryst. Growth 274, 638–652.

Kappadan, S., Gebreab, T.W., Thomas, S., Kalarikkal, N., 2016. Tetragonal $BaTiO_3$ nanoparticles: an efficient photocatalyst for the degradation of organic pollutants. Mater. Sci. Semicond. Process. 51, 42–47.

Kosmulski, M., 2009. pH-dependent surface charging and points of zero charge. IV. Update and new approach. J. Colloid Interface Sci. 337, 439–448.

Kuan, W.H., Chen, C.Y., Hu, C.Y., Tzou, Y.M., 2013. Kinetic modeling for microwave enhanced degradation of methylene blue using manganese oxide. Int. J. Photoenergy. https://doi.org/10.1155/2013/916849.

Kurniawan, T.A., Lo, W.H., Chan, G., 2006a. Degradation of recalcitrant compounds from stabilized landfill leachate using a combination of ozone-GAC adsorption treatment. J. Hazard Mater. 137, 443–455.

Kurniawan, T.A., Lo, W.H., Chan, G., 2006b. Radicals-catalyzed oxidation for degradation of recalcitrant compounds from landfill leachate. Chem. Eng. J. 125, 35–57.

Kurniawan, T.A., Lo, W.H., 2009. Removal of refractory compounds from stabilized landfill leachate using an integrated H_2O_2 oxidation and granular activated carbon adsorption treatment. Water Res. 43, 4079–4091.

Kurniawan, T.A., Lo, W.H., Chan, G., Silanpa, M., 2010. Biological processes for treatment of landfill leachate. J. Environ. Monit. 12, 2032–2047.

Kurniawan, T.A., Lo, W.H., Chan, G., Silanpa, M., 2011. Nano-adsorbents for remediation of aquatic environment: local and practical solutions for global pollution problems. Crit. Rev. Environ. Sci. Technol. 42, 1233–1295.

Kurniawan, T.A., Lin, Y.Y., Tong, O., Albadarin, A.B., Walker, G., 2018. $BaTiO_3/TiO_2$ composite-assisted photocatalytic degradation for removal of acetaminophen from synthetic wastewater under UV-vis irradiation. Mater. Sci. Semicond. Process. 73, 42–50.

Lacerda, L.H.S., de-Lazaro, S.R., 2016. A theoretical investigation of the Zn-doping influence on structural and electronic properties of $BaTiO_3$. Solid State Ion. 297, 36–42.

Li, J., Ko, J.W., Ko, W.B., 2015. Synthesis of $BaTiO_3$-TiO_2-Graphene nanocomposites and kinetics studies on their photocatalytic activity. Eurasian Chem. Technol. J. 17, 281–286.

Li, L.L., Fan, L.L., Sun, M., Qiu, H.M., Li, X.J., Duan, H.M., Luo, C.N., 2013a. Adsorbent for hydroquinone removal based on graphene oxide functionalized with magnetic cyclodextrin-chitosan. Int. J. Biol. Macromol. 58, 169–175.

Li, R., Li, Q.Y., Zong, L.L., Wang, X.D., Yang, J.J., 2013b. $BaTiO_3/TiO_2$ heterostructure nanotube arrays for improved photoelectrochemical and photocatalytic activity. Electrochim. Acta 91, 30–35.

Lin, Y.Y., Kurniawan, T.A., Yi, Z., Albadarin, A., Walker, G., 2017. Enhanced photocatalytic degradation of acetaminophen from wastewater using $WO_3/TiO_2/SiO_2$ composite under UV-VIS irradiation. J. Mol. Liq. 243, 761–770.

Lin, Y.Y., Kurniawan, T.A., Zhu, M.T., Ouyang, T., Avtar, R., Othman, H.D., Balsam, M., Albadarin, A., 2018a. Removal of acetaminophen from synthetic wastewater in a fixed-bed column adsorption using low-cost coconut shell waste pretreated with NaOH, HNO_3, ozone, and/or chitosan. J. Environ. Manag. 226, 365–376.

Lin, Y.Y., Kurniawan, T.A., Albadarin, A., Walker, G., 2018b. Enhanced removal of acetaminophen from synthetic wastewater using multi-walled carbon nanotubes (MWCNT) chemically modified with NaOH, HNO_3/H_2SO_4, ozone, and/or chitosan. J. Mol. Liq. 251, 369–377.

Liu, G.G., Han, K., Ye, H.Q., Zhu, C.Y., Gao, Y.P., Liu, Y., Zhou, Y.H., 2017. Graphene oxide/triethanolamine modified titanate nanowires as photocatalytic membrane for water treatment. Chem. Eng. J. 320, 74–80.

Liu, L.P., Zhang, Y.H., Lv, F.Z., Tong, W.S., Ding, L., Chu, P.K., Li, P.G., 2016. Polyimide composites composed of covalently bonded $BaTiO_3$@GO hybrids with high dielectric constant and low dielectric loss. RSC Adv. 6, 86817–86823.

Luan, J.F., Hu, Z.T., 2012. Synthesis, property characterization, and photocatalytic activity of novel visible light-responsive photocatalyst Fe_2BiSbO_7. Int. J. Photoenergy. https://doi.org/10.1155/2012/301954.

Luan, X., Wing, M.T.G., Wang, Y., 2015. Enhanced photocatalytic activity of graphene oxide/titania nanosheets composites for methylene blue degradation. Mater. Sci. Semicond. Process. 30, 592–598.

Mohtora, N.M., Othman, H.D., Bakarb, S.A., Kurniawan, T.A., Dzinuna, H., Norrdina, M.N.A.M., 2018. Synthesis of nanostructured titanium dioxide layer onto kaolin hollow fiber membrane via hydro-thermal method for decolorisation of reactive black 5. Chemosphere 208, 595–605.

Meyer, J.C., Geim, A.K., Katsnelson, M.I., Novoselov, K.S., Booth, T.J., Roth, S., 2007. The structure of suspended graphnen sheet. Nature 446, 60–63.

Nageri, M., Kumar, V., 2018. Manganese-doped $BaTiO_3$ nanotube arrays for enhanced visible light photocatalytic applications. Mater. Chem. Phys. 213, 400–405.

Nguyen-Phan, T.D., Pham, V.H., Shin, E.W., Pham, H.D., Kim, S., Chung, J.S., Kim, E.J., Hur, S.H., 2011. The role of graphene oxide content on the adsorption-enhanced photocatalysis of titanium dioxide/graphene oxide composites. Chem. Eng. J. 170, 226–232.

Ong, Y.P., Ho, L.N., Ong, S.A., Banjuraizah, J., Ibrahim, A.H., Lee, S.L., Nordin, N., 2019. A synergistic heterostructured ZnO/$BaTiO_3$ loaded carbon photoanode in photocatalytic fuel cell for degradation of Reactive Red 120 and electricity generation. Chemosphere 219, 277–285.

Oz, M., Lorke, D.E., Hasan, M., Petroianu, G.A., 2011. Cellular and molecular actions of methylene blue in the nervous system. Med. Res. Rev. 31, 93–117.

Ramezanpour, S., Sheilhahoaie, I., Khatamian, M., 2018. Constructing Mn_3O_4/Cu hybrid nanorods as superior photocatalyst. Nanostruct. Nanoobjects 16, 396–402.

Ran, J., Guo, M.J., Zhong, L., Fu, H.Q., 2019. In situ growth of $BaTiO_3$ nanotube on the surface of reduced graphene oxide: a lightweight electromagnetic absorber. J. Alloy. Comp. 773, 423–431.

Ray, S.K., Dhakal, D., Kshetri, Y.K., Lee, S.W., 2017. Cu-alpha-$NiMoO_4$ photocatalyst for degradation of methylene blue with pathways and antibacterial performance. J. Photochem. Photobiol., A 348, 18–32.

Rezakazemi, M., Kurniawan, T.A., Albadarin, A.B., Shirazian, S., 2018. A molecular modeling investigation on the mechanism of phenol removal from aqueous media by single-walled and multi-walled carbon nanotubes. J. Mol. Liq. 271, 24–30.

Sabarish, R., Unnikrishnan, G., 2018. Novel biopolymer templated hierarchical silicalite-1 as an adsorbent for the removal of rhodamine B. J. Mol. Liquids 272, 919–929.

Sahu, K., Choudhary, S., Khan, S.A., Pandey, A., Mohapatra, S., 2019. Thermal evolution of morphological, structural, optical and photocatalytic properties of CuO thin films. Nanostruct. Nanoobjects 17, 92–102.

Saquib, M., Muneer, M., 2003. TiO_2-mediated photocatalytic degradation of a triphenylmethane dye (gentian violet), in aqueous suspensions. Dyes Pigments 56, 37–49.

Sharma, M., Behl, K., Nigam, S., Joshi, M., 2018. TiO_2-GO nanocomposite for photocatalysis and environmental applications: a green synthesis approach. Vacuum 156, 434–439.

Sillanpaa, M., Kurniawan, T.A., Lo, W., 2011. Degradation of chelating agents in aqueous solution using advanced oxidation process (AOP). Chemosphere 83, 1443–1460.

Singh, R., Dutta, S., 2019. The role of pH and nitrate concentration in the wet chemical growth of nano-rods shaped ZnO photocatalyst. Nanostruct. Nanoobjects 18, 100250.

Su, S.S., Liu, Y.Y., Liu, X.M., Jin, W., Zhao, Y.P., 2019. Transformation pathway and degradation mechanism of methylene blue through beta-FeOOH@GO catalyzed photo-Fenton-like system. Chemosphere 218, 83–92.

Szabo, T., Berkesi, O., Forgo, P., Josepovits, K., Sanakis, Y., Petridis, D., Dekany, I., 2006. Evolution of surface functional groups in a series of progressively oxidized graphite oxides. Chem. Mater. 18, 2740–2749.

Tao, H., Liang, X., Zhang, Q., Chang, C.T., 2015. Enhanced photoactivity of graphene/titanium dioxide nanotubes for removal of acetaminophen. Appl. Surf. Sci. 324, 258–264.

Utara, S., Hunpratub, S., 2018. Ultrasonic assisted synthesis of $BaTiO_3$ nanoparticles at 25 °C and atmospheric pressure. Ultrason. Sonochem. 41, 441–448.

Vasilaki, E., Georgaki, I., Vernardou, D., Vamvakaki, M., Katsarakis, N., 2015. Ag-loaded TiO_2/reduced graphene oxide nanocomposites for enhanced visible-light photocatalytic activity. Appl. Surf. Sci. 353, 865–872.

Vig, A.S., Gupta, A., Pandey, O.P., 2018. Efficient photodegradation of methylene blue (MB) under solar radiation by ZrC nanoparticles. Adv. Powder Technol. 29, 2231–2242.

Wang, M., Yang, J.Z., Wang, H.T., 2001. Optimisation of the synthesis of a watersoluble sulfur black dye. Dyes Pigments 50, 243–246.

Wang, M.Y., Zhu, W., Zhang, D.E., Li, S.A., Ma, W.X., Tong, Z.W., Chen, J., 2014. CeO_2 hollow nanospheres decorated reduced graphene oxide composite for efficient photocatalytic dye-degradation. Mater. Lett. 137, 229–232.

Wang, R.X., Zhu, Q., Wang, W.S., Fan, C.M., Xu, A.W., 2015. $BaTiO_3$-graphene nanocomposites: synthesis and visible light photocatalytic activity. New J. Chem. 39, 4407–4413.

Wang, Y., Niu, J.F., Zhang, Z.Y., Long, X.X., 2008. Sono-photocatalytic degradation of organic pollutants in water. Prog. Chem. 20, 1621–1627.

Wolski, L., Ziolek, M., 2018. Insight into pathways of methylene blue degradation with H_2O_2 over mono and bimetallic Nb, Zn oxides. Appl. Catal. B Environ. 224, 634–647.

Xu, M.S., Liang, T., Shi, M.M., Chen, H.Z., 2013. Graphene-like two-dimensional materials. Chem. Rev. 113, 3766–3798.

Yan, J., Fan, Z.J., Wei, T., Qian, W.Z., Zhang, M.L., Wei, F., 2010. Fast and reversible surface redox reaction of graphene-MnO_2 composites as supercapacitor electrodes. Carbon 48, 3825–3833.

Yang, J., Chen, C.C., Ji, H.W., Ma, W.H., Zhao, J.C., 2005. Mechanism of TiO_2-assisted photocatalytic degradation of dyes under visible irradiation: photoelectrocatalytic study by TiO_2-film electrodes. J. Phys. Chem. B 109, 21900–21907.

Yang, L., Xu, L., Bai, X., Jin, P.K., 2019. Enhanced visible-light activation of persulfate by Ti^{3+} self-doped TiO_2/graphene nanocomposite for the rapid and efficient degradation of micropollutants in water. J. Hazard Mater. 365, 107–117.

Yao, Y.J., Xu, C., Qin, J.C., Wei, F.Y., Rao, M.N., Wang, S.B., 2013. Synthesis of magnetic cobalt nanoparticles anchored on graphene nanosheets and catalytic decomposition of orange II. Ind. Eng. Chem. Res. 52, 17341–17350.

Zhai, L.L., Bai, Z.S., Zhu, Y., Wang, B.J., Luo, W.Q., 2018. Fabrication of chitosan microspheres for efficient adsorption of methyl orange. Chin. J. Chem. Eng. 26, 657–666.

Zhang, Y.H., Zhang, N., Tang, Z.R., Xu, Y.J., 2012. Graphene transforms wide band gap ZnS to a visible light photocatalyst, the new role of graphene as a macromolecular photosensitizer. ACS Nano 6, 9777–9789.

Zhao, J.C., Chen, C.C., Ma, W.H., 2005. Photocatalytic degradation of organic pollutants under visible light irradiation. Top. Catal. 35, 269–278.

Zhao, Y.J., Zhang, X.W., Liu, J.L., Wang, C.Z., Li, J.B., Jin, H.B., 2018. Graphene oxide modified nano-sized $BaTiO_3$ as photocatalyst. Ceram. Int. 44, 15929–15934.

Zheng, H.J., Zhu, K.J., Wu, Q.L., Liu, J.S., Qiu, J.H., 2013. Preparation and characterization of monodispersed $BaTiO_3$ nanocrystals by sol-hydrothermal method. J. Cryst. Growth 363, 300–307.

Zhu, X.D., Castleberry, S.R., Nanny, M.A., Butler, E.C., 2005. Effects of pH and catalyst concentration on photocatalytic oxidation of aqueous ammonia and nitrite in titanium dioxide suspensions. Environ. Sci. Technol. 39, 3784–3791.